Stabilizing wide bandwidth, tuning fork detected force feedback with nonlinear interactions

C. L. Jahncke* and H. D. Hallen

North Carolina State University, Raleigh, NC 27695-8202

*St. Lawrence University, Canton, NY 13617

Near-field scanning optical microscope (NSOM) force feedback can be de-stabilized by the anisotropy in response times engendered by nonlinear tip sample interactions. This nonlinear interaction, the tapping of the tip on layers adsorbed on the sample, is important when the intrinsic damping of the system is low. We present strong evidence of tapping on adlayers rather than the sample surface at operational distances, and numerically solve a model to find the dynamics of tip motion. These novel results illuminate the origins of feedback problems when using tuning fork detection of oscillation amplitude, and show an optimal technique that uses the rapid response of the tip-adlayer nonlinearity to circumvent the slow damping response and enable wide bandwidth, stable distance regulation for these systems.

(07.79.-v, 07.79.Fc, 68.37.-d, 68.37.Uv, 68.60.-p)

Introduction

Near-field scanning optical microscopes (NSOMs) enable the extension of many standard optical techniques to higher resolution imaging. Examples include spectroscopy,[1-9] fluorescence,[10-12] optical carrier lifetime, [13, 14] and optical beam-induced current measurement.[15, 16] Often the benefits extend beyond simply resolution enhancement. Near-field Raman spectroscopy exhibits surface enhancement, reduced Rayleigh tails and new selection rules compared to far-field Raman.[8, 17] A relative of Raman spectroscopy, Gradient-field Raman,[18] must be invoked to fully explain the spectra, which includes lines from vibration modes not observed with far-field Raman in any geometry. Fluorescence lifetime can be adjusted by the probe position.[10] The metal aperture can be used as a tunnel electrode for injecting current to drive electromigration. [19, 20] The tip is brought close to the surface for electromigration, then retracted by a few nanometers for optical imaging to quantify the electromigration. All these measurements, especially the latter three, require precise positioning of the probe relative to the sample, with well-characterized distance control. For example, quantification of the nano-Raman signal with distance provides a signature for the mechanism of selection rule modification. In this paper, we explore a technique to enhance the force feedback distance regulation scheme widely used in NSOM.

Description of Force Feedback Methods

Distance control in NSOM has evolved significantly over the past 15 years. Early NSOMs [21, 22] did not have distance control at all, but often imaged at different distances from the sample until the tip was so close that it crashed into the surface. These

early practitioners tried several distance regulation schemes without general success. These schemes included capacitance feedback and tunnel current (as in scanning tunneling microscopy, STM) feedback. Two systems of lateral force feedback were independently introduced as the first general-purpose distance regulation methods. The pin-hole method [23] used optical lever-arm amplification of the lateral motion of the tip, detected by the variation in intensity of light coupled through a pinhole in the back focal plane of the light detection optics, to determine distance. The probe tip was oscillated laterally at its resonant frequency, and the light through the pinhole detected coherently with a lock-in amplifier. The amplitude of oscillation decreases as the tip approaches the surface, due to interactions with the surface. The distance over which the amplitude varies is approximately 5-20 nm, almost independent of the materials system, from ambient to submersed in superfluid helium. [4] The other early general-purpose distance regulation method involved interferometry to measure the magnitude of the resonant probe vibration. [24, 25] Light shone on the side of the probe was split into two beams with a Wollaston prism, reflected from the probe at two distances along its length, and recombined to form an interference pattern proportional to the amount of tip bending. Coherent lock-in detection at the resonance and twice the resonance frequency was used to make the output independent of fluctuations in the light intensity. The same broadly applicable properties of the probe vibration amplitude variation with distance apply to this technique as to the above.

Key properties of these two techniques: lever arm amplification of the tip motion from the former, laser illumination of the side from the latter, and piezoelectric-driven oscillation of the probe at resonance from both, were combined to create the NSOM force

feedback scheme that was the standard for many years. Laser light was focused near the side of the probe (10's of microns from the tip), and the motion of the diffraction pattern detected either with a split photodiode or edge detection on the other side of the microscope. Fiber probes were mounted with approximately 2 mm extending beyond the mount so that the resonant frequency of this beam was ~60-70 kHz. This could be estimated from uniform bending beam formulae, or more accurately by accounting for the taper.[26] The signal was independent of the optical microscopy signal. It could be used either in microscopes that scanned the sample, [23] or those that scanned the tip.[27] The primary disadvantages were the stray light due to the laser illumination and the adjustments required at every tip replacement: the focal point of the light had to be positioned relative to the fiber probe tip, and the detector had to be moved to the edge of a diffraction feature, often by scanning the detector to maximize the signal amplitude. The light used for distance regulation could sometimes affect the optical measurement, by exciting carriers in a semiconductor sample, for example. Such considerations gave rise to several non-optical-based probe oscillation amplitude detection methods. Many of these are still in use today. They include detection of the back-force of the probe on the driving piezoelectric through impedance changes of the driver at the probe resonance frequency, [28-30] detection of the probe oscillation with a matched oscillator and detector method,[31] and the primary method currently in use,[32] which relies on voltage generation by a tuning fork to measure the oscillation amplitude.

Bandwidth Limitations and Solutions

In the tuning fork feedback scheme, the fiber is glued to one arm of the tuning fork and is driven at the resonance frequency of the tuning fork and probe system. The bare tuning fork resonance is usually 32,768 Hz, but this is typically increased to 34-40 kHz when the fiber is bonded to one tuning fork arm due to stiffening of the mechanical oscillator. The resonance frequency of the fork/fiber can decrease due to a poor glue joint or too much fiber extending past the arm of the tuning fork. This length of fiber should be short so that the resonance frequency of the fiber alone is higher than the tuning fork/fiber assembly. The important point for this paper is that the resonance frequency is significantly less than the 60-70 kHz used in the optical lever arm and other non-optical feedback schemes currently in use, and the quality factors, Q, are often higher with useful Q's up to 700. Since the intrinsic probe time constant scales with the width of the resonancepeak or Q/resonance frequency, the time constant is much larger for the tuning fork feedback as compared to previously used optical feedback and, therefore, the time response is slower. By contrast, the nonlinear interaction (discussed in more detail below) between the tip and sample (or adlayers) results in a rapid decrease in oscillation amplitude when the probe is close to the surface. The difference in response times is much more disparate with the tuning fork detection than when using the fiber resonance, so this disparity has not been a significant issue with optical-based amplitude detection systems.

Evidence of this limited bandwidth and contrasting response times is typified by the low frequency, asymmetric oscillations that occur as the feedback gain is increased. These oscillations are shown in the trace of tip position vs. time (with the probe *not*

scanned laterally) observed in figure 1. When the probe is relatively far from the sample, the high Q combined with the relatively low resonant frequency results in a slow intrinsic time response (ITR) of the oscillator. In particular, the oscillator has a long 'ring-down' time. Alternately, when the probe is close to the surface, the tapping-like interaction between the probe and the surface or surface adlayers rapidly decreases the oscillation amplitude. [33, 34, 35] We refer to this as the tapping time response or TTR. The frequency of these oscillations is roughly the width of the resonance curve, as expected. When the probe is close to the surface, the rapid TTR pulls the probe back. The probe amplitude slowly grows due to the ITR or width or the resonance curve causing an overshoot. This brings the probe far from the surface, and the response time is now dominated by the ITR, so the probe slowly returns toward the surface and the cycle starts over. The inequality of the response in the two places makes adjustment of the feedback precarious. In fact, a linear feedback system, as is universally used, is not appropriate. The feedback can be stabilized and the oscillation removed by setting the feedback loop response to work only at frequencies for which the slower process can respond. This is limiting, however, since the bandwidth of the feedback would then be the same as the frequency width of the resonance peak, between 20-100 Hz, which is too slow for desired imaging rates in most cases. Another remedy is to damp the resonance so that Q is reduced and the resonance peak width increases. This is not optimal either, since the reduced peak height impairs low noise topographic imaging.

To enhance the bandwidth of operation we take advantage of the sample-probe nonlinear interaction to increase the response rate of the oscillation amplitude when the probe retracts from the surface. To understand how our method works, note that there are

two components that result in a reduction of the signal when in feedback: the frequency shift and the overall reduction of the peak due to decreasing Q as the tip approaches the surface. Both of these effects can be seen in the resonance curves shown in figure 2a. As the setpoint is decreased, the resonance frequency increases and the quality factor decreases resulting in a reduced signal at resonance. If we set the driving frequency below the resonance frequency, and attain feedback, two things happen. The oscillation damps and the resonance frequency increases. Both result in a decrease in oscillation amplitude and both are rapid responses. Similarly when the sample retracts from the probe, i.e. the probe falls off a ledge, the oscillation begins to grow for two reasons -- a decrease in damping and a shift in the resonance frequency. In this probe-motion direction, however, the growth in the oscillation amplitude due to the decrease in damping is slow due to the ITR, the slow Q response, but the oscillation rapidly grows due to the shift of the resonance frequency back towards its free oscillation value. The latter mechanism dominates, and the response is fast. This same process works on the high frequency side of the peak due to the 180 phase change in the signal from the tuning fork so that the slope of the resonance curve is upwards on both sides of the resonance. We use the X output from a lock-in amplifier to sense the tuning fork signal so that we are sensitive to the phase, since X is the in phase component of the resonance signal. Therefore, the operating frequency can be tuned until the response rate is the same in the two directions, so the linear feedback loop can effectively control the distance. This does not significantly reduce the sensitivity of the detection, and allows wide bandwidth operation. Operating off resonance results in a lower signal and, therefore, lower signal to noise ratio. However, typical driving frequencies occur at about 75-85% of the peak

height resulting in a 25-15% reduction in signal with a factor of four or more improvement in bandwidth, so the tradeoff is favorable. In principle, this procedure benefits tuning-fork detection of vertical tapping mode force feedback [36, 37] in the same manner.

Results and Discussion

We study the time response of the probe as a function of driving frequency by performing three experiments. 1) We turn up the gain until the system just oscillates, and we measure the oscillation amplitude with a fixed high feedback electronics gain as a function of driving frequency (position on the resonance curve). 2) We measure the overshoot response of the system when the probe is given an impulse alternately pushing it towards and pulling it away from the surface as a function of driving frequency with a fixed feedback gain. Finally we look at the time response of the system to a ramp function optimizing the gain at each driving frequency.

In the first experiment, we increase the gain enough to cause the system to oscillate, as seen in figure 1. We monitor the amplitude of these oscillations as a function of driving frequency, and find a reduction in the oscillation amplitude on both the high frequency and low frequency sides of the resonance as a result of an improvement in the time response, figure 3. As we move off resonance, the frequency shift due to the tapping becomes the more dominant mechanism (TTR), and the system is able to respond more rapidly. On resonance the response is dominated by the high quality factor (ITR) and responds slowly resulting in large oscillation amplitudes. The time constant that results from these two mechanisms is $(1/TTR + 1/ITR)^{-1}$.

In the second experiment, the probe is placed in feedback and a pulse is applied to the z-piezo causing the sample to move alternately towards and away from the probe. We repeat this for a variety of driving frequencies while we keep the gain constant (figure 4). When the pulse pushes the probe toward the surface, the tapping force increases, and the tip pulls back rapidly overshooting the desired signal level at or near the resonance frequency. This results in a decrease in tapping, and the system slowly moves the probe toward the surface. This behavior can be seen in the black lines in figure 4 near resonance. In this case the system response is initially dominated by the fast TTR so the probe moves out rapidly, but it overshoots due to the slow, ITR, response of the high Q of the probe/fork. The slow response continues to dominate as the probe is returned to the surface. As the driving frequency is increased past the resonance frequency, we see the time response improves (due to the TTR), and the overshoot decreases. Alternately, when the probe is pulled away from the surface, as seen in the gray lines in figure 4, the time response for the probe to find the surface is again dominated by the slow, ITR, response of the high Q of the probe/fork. As the driving frequency is increased past resonance, we see the time response improves as indicated by the sharpening of the line for the inward motion (the decrease in the time it takes the probe to find the surface) and a lack of overshoot for the outward motion. The important point for improving the bandwidth of the experiment is that on the high frequency side of the resonance the time it takes for the probe to move in the two directions align.

To investigate this behavior further we apply a trapezoidal shaped pulse to the z-piezo with a rise time and a fall time of 8 msec leaving enough time in between for the system to settle. We optimize the gains while preventing the overshoot that we see in

figure 4. The response of the feedback loop to the pulse can be seen in figure 5. Note that once again, the time for the inward and outward motion of the probe align on the high frequency side of the resonance. We can understand this data better by plotting the time for the inward motion as a function of driving frequency, figure 6a. The overall time it takes for the probe to find the surface depends on the size of the ramp and time constant for the ramp, but we note that the shape of this curve is similar to the curve for the oscillation amplitude shown in figure 3. In each experiment, figures 3, 4, 5, and 6a), we see that the time response of the probe improves dramatically on the high frequency side of the resonance peak. To understand this improvement we look at the mathematical model for the tapping interaction.

Tapping Interaction

The tuning fork/probe is a driven damped harmonic oscillator. We can model the tapping force as the addition of a strong force when the lateral position of the tip exceeds a critical value [33,38]. The same model applies whether the probe is tapping on the sample surface adlayers or on the sidewalls of a cavitation hole in the adlayers. Only the interpretation of the critical position, $\mathbf{x_c}$, changes from the distance to touch the surface to the distance to reach the edge of the cavity. The equation that describes such a system with effective mass m_{eff} driven by a force F_{drive} is

$$F_{drive}/m_{eff} = F_0\cos(\omega_d t)/m_{eff} = \ddot{x} + 2\beta_0\dot{x} + \omega_0^2 x + H(x-x_c)[\,\omega_1^2 (x-x_c) + 2\beta_1\dot{x}]\,, \qquad \textbf{(1)}$$

where ω_d is the radial tip oscillation driving frequency, β_0 and β_1 refer to damping and ω_0 and ω_1 the resonance frequencies of the fork/fiber oscillator and fiber/adlayer system,

respectively, and H is the step function. The β_0 and ω_0 terms are determined from the resonance curve far from the surface. F_0/m_{eff} is set to normalize the oscillation amplitude to 1. We determine ω_1 and β_1 using a damped resonance curve just before clamping. The clamped resonance occurs when the probe strongly taps the surface of the sample (not the adlayers) and is indicated by a very large shift in the resonance frequency (≥400 Hz for our probes.) We will discuss this in more detail later in this paper. Others have modeled the tip sample interaction with a probe bending model that includes elastic and frictional forces [39] and a viscous damping model[40]. In each case they adjust at least two free parameters for each resonance curve. The tapping model discussed here has the advantage that all of the resonance curves can be reproduced with two free parameters in total. Figure 2b shows the resonance curves calculated using the model and their agreement with the resonance curves we found experimentally in Figure 2a, indicating that the model accurately describes our system.

We now use the model to understand the dynamics of the system. For a variety of driving frequencies, we solve equation (1) numerically in the following way. We use the Mathematica NDSolve Algorithm to find x(t) without tapping ($\omega_1 = \beta_1 = 0$), and wait for the solution to reach steady state. Next we add in the tapping term and look at the 1/e time for the signal to settle. We call this tapping on (analogous to TTR on). Alternately, we let the system settle with the tapping term included, then remove the tapping term and obtain the 1/e rise time. We call this tapping off (analogous to TTR off). The results can be seen in figure 6b. The time response near resonance is slow because the system is dominated by the high Q of the probe, ITR. The time response away from resonance is faster due to the frequency shift of the resonance peak. The difference in the time

response at resonance between the tapping on and tapping off is analogous to the difference in time response when the probe is dominated by the tapping interaction (TTR, tapping on) versus the time response when the probe is dominated by the damping (ITR, tapping off). It is important to note that the time response determined by the model is consistent with data from the experiments. We see improved time response on both the high and low frequency side of the resonance curve. We see the worst time response just below resonance, and we see that the time response aligns on the high frequency side of the resonance curve. Clearly the driving frequency where the time response aligns is the best choice for increased bandwidth operation.

Guide for Practitioners

There are several ways that the best drive frequency can be determined. Our results apply to the case generally encountered in NSOM: the oscillation amplitude is small (a few nanometers or less) and ambient operation of an NSOM (room temperature, solid sample). The optimal driving frequency occurs at about 75% of the peak amplitude on the high frequency side of resonance. Large setpoints (80 to 90 percent) provide better signal to noise and reasonable time response. An alternative method to determine the proper operating frequency when not under standard operating conditions is to use the same experiments presented in this paper. First, the optimal driving frequency is determined by applying a pulse to the z piezo, while observing the time response of the in and out motion of the tip as a function of driving frequency. Choose the frequency where the time response for the two directions becomes the same. Second, a damped resonance

curve indicates that the best operating frequency is just before the damped curve crosses over the undamped resonance curve. This procedure does not need to be repeated for every new sample and probe. The primary effect of the sample will be in determining the damping and the spring constant which will affect β_1 and ω_1 respectively in the formula above. However, for a given sample type, this parameter should remain fairly constant. Optimizing the drive frequency should occur at least once for each type of sample.

Each time the probe is changed, and occasionally as the glue on the probe assembly dries, the resonant frequency and the quality factor, Q, change -- potentially modifying the optimal driving frequency. We used the model to study the effect of each of these parameters on the choice of drive frequency. We found that changing the resonance frequency of the probe does not change the overall curve shape, and the damped curve crosses the resonance curve at the same percentage of the peak height in each case. In figure 7 the free and 85% damped resonance curves are shown for three different resonance frequencies, 39524 Hz, 35931 Hz, and 32328 Hz, normalized to the center frequency; the curves lie right on top of each other. Figure 8 shows the effect of changing the Q of the probe/fork on the resonance curves for two different Q values, 630 and 315. In the figure, the resonance curves are normalized for ease of comparison, and the free resonance curve and two damped curves (75% and 85% of peak) are shown for each Q-value. Again, we find that the damped resonance curve crosses the undamped curve in almost the same place in terms of percent of peak height, however, the curve shape changes as well. When we examine this more closely by looking at the time response (figure 9) as a function of Q, we find that for lower Q values, there is a larger range of frequencies available for operation. However, the optimal choice for drive

frequency still occurs just before the damped resonance curve crosses the free resonance curve, which is still at approximately the same percentage of the peak height (~75%) regardless of Q value or resonance frequency.

Tip-Sample Interaction

A very important point in all of our considerations here is that we have a small tip oscillation amplitude. We measure our probe amplitudes to be 0.5 to 2 nm by stepping the oscillating fiber through a Gaussian beam and looking at the ratio of the Gaussian signal (DC) to its derivative signal at the fiber resonance (AC), a technique described by Wei, Wei, Fann[41]. This small oscillation amplitude results in a small voltage signal from the tuning fork which has a high driving impedance (electrically it is a ~1 pF capacitor). As a result, care must be taken to insure that the signal reaches the preamplifier without attenuation. We use driven guard shields to reduce the capacitance load that the tuning fork must drive, and we use a preamplifier with guarded inputs and a high input impedance (high resistance $10^8\Omega$, low capacitance 1pF)[42]. We measure a signal of 10's of microvolts from the background to the peak using our scheme. Our preamp has a gain of 100 resulting in a signal in the millivolt range at the lock-in amplifier input. The oscillator piezo is driven at a few millivolts to create a resonance amplitude of ~1 nm with the probe retracted from the surface.

Our approach curves (figure 10), the change in amplitude of vibration as a function of distance towards the sample, indicate that the range of tip-sample interaction is approximately an order of magnitude larger than the lateral amplitude of vibration of our probe. This contradicts the idea that the tip taps the sample surface because the

oscillation amplitude is not large enough to reach it; it supports the idea that the probe interacts with surface adlayers. Note that we refer to the sample as the solid surface beneath the adlayers. If the tip were tapping the surface, the tip-sample interaction distance would need to be less than or equal to the lateral vibration amplitude, depending upon the angle of deviation from square and zero if the tip vibrated parallel to the surface. The approach curves shown in figure 10 are for a sample that is deliberately tilted at an angle of ~24° (66° angle between probe and surface), so that the change in the interaction distance as the probe oscillation amplitude is increased can be seen.

Further evidence that the probe is interacting with surface adlayers rather than the surface itself is found in the resonance curves. As we mentioned earlier, for our model we determine ω_1 and β_1 using a damped resonance curve <u>just before</u> clamping. Clamping occurs when the probe jumps to contact the sample surface. When viewing resonance curves, this jump to contact is indicated by a very large shift in the resonance frequency (≥400 Hz for our probes) as can be seen in figure 11. Gregor et. al [33] use the clamped resonance curve to find the values for β_1 and ω_1 to model their low temperature experiments, and they find that it accurately describes their resonance curves as they approach the sample. In our experiments, the clamped mode has a much higher spring constant than we find in normal operation, and the use of its parameters does not fit the resonance curve data. This indicates that in normal operation we are not tapping on the sample surface, as Gregor is (Gregor's adlayers are very stiff since they are frozen, so are similar to our sample surface), rather we are tapping on softer adlayers or cavitation sidewalls in the adlayers. We do not know the composition of the adlayers that we tap on, although it obviously depends upon the nature of the surface, hydrophobic or

hydrophilic, and the history of the sample. One obvious candidate is water. Water is structured [43] near a hydrophilic surface, as are other near-surface solvents [44]. Hydrophilic surfaces also tend to have a high surface energy, so organic molecules in the air are likely to stick when they impinge on the surface. Evidence that water is involved is given by Wei and Fann[45], who measured the force feedback signals as a function of distance for several different humidity levels. Our model is applicable when cavitation is present. We believe that cavitation is likely for the reduced mobility layers near the surface and with the ultrasonic tip oscillation frequency. Cavitation is also possible with less mobile adsorbates and the less structured water (clathrates) near a hydrophobic surface [46]. Either case, tapping on the adlayers or cavitating in them, is consistent with our observation of the change in stiffness that we observe when the probe reaches the sample surface. A closer examination of the approach curves shown in figure 10 reveals at least two distinct regions. For the curves shown, the first region, labeled A, shows that the amplitude of the feedback signal decreases slowly as the probe moves towards the surface (~15% in 10+ nm). The second region, labeled B, shows a much sharper decrease in feedback signal (~80% in 2 to 5 nm). These two regions can be understood by examining the resonance curve shift as a function of setpoint (or fraction of resonance peak amplitude), figure 12. The resonance curve does not shift very much (a few hertz) until the region between 70% and 80% of the peak frequency at which point the resonance begins to shift rapidly (10's of hertz). There is arguably even a third region where the probe is clamped which is accompanied by an even larger frequency shift (100's of hertz).

In Wei and Fann's investigation of the effect of relative humidity (RH), we find that their resonance curves as a function of tip sample separation show similar behavior to our resonance curves (figure 2) for low values of RH. However, for the case of large RH, 80%, they do not observe a blueshift of the resonance curve until they are only a few nm from the surface. This would indicate that tapping is not the dominant force interaction prior to this point. There are several explanations for their observations that are consistent with our model of tapping on cavitation side-walls. First, it is possible that our adlayers are organics, while theirs are water, and the water may have too low a viscosity to support cavitation until they are only a few nm thick. Second, the higher RH case has a thicker layer of water, which may wick up onto the sides of the fiber preventing cavitation. (This explanation seems unlikely.) Finally, it is only the thin layers of water (few nm) are ordered and viscous enough to allow cavitation. In the case of high RH, only a fraction of the adlayer would support cavitation. It is worth noting that the shape of our approach curves (figure 10) are similar to Wei and Fann's approach curves in higher RH. The slope of region A is lower and the transition region is more rounded than the low RH case. However, we do observe tapping behavior (blue shifted resonance curves, figure 12) in region A as well as B.

Additionally, we note that we measure tunnel current between the probe and the surface in our electromigration studies, [19, 20] and have found no tunnel current in normal operation. We must set the feedback level quite low to obtain tunnel current for the electromigration. The current again falls to zero as we pull back for NSOM imaging. The process is repeatable, with minimal wear indicated by little change in resolution even after several hours at a low feedback level (tunneling). These experiments are consistent

with the notion that at the top portion of the approach curve, the probe is not interacting with the sample surface but rather with the surface adlayers.

Conclusions

The resonance frequency shift we see implies that a nonlinear mechanism is active. We have modeled and measured the dynamic response of the probe, including the nonlinearity of the tip-sample interaction. This model has led to a method to increase the response rate of the high Q tuning-fork-based distance regulation system without overly damping the quality factor of the oscillator. The method is based on the careful choice of operating frequency, and an algorithm is given to find that operating point as determined by our understanding of the oscillator system. The probe taps on surface adsorbed layers rather than the surface, as indicated by our tunnel current studies, analysis of length scales, and nonlinear resonance frequency shifts, so the force feedback should be an accurate measure of distance from the surface for typical oscillation amplitudes that are much smaller than the approach curve distance.

Acknowledgments

This work was supported by the National Science Foundation through grant DMR-9975543 and the Research Corporation through grant CC5342. We thank Brian Watson for useful conversations.

References

[1] E. Betzig and J.K. Trautman, Science **257**, 189 (1992).

[2] H. D. Hallen, A. H. La Rosa and C. L. Jahncke, Phys. Stat. Sol. (a) **152**, 257 (1995).

[3] H. F. Hess, E. Betzig, T. D. Harris, L. N. Pfeiffer and K. W. West, Science **266**, 1740 (1994).

[4] R. D. Grober, T. D. Harris, J. K. Trautman, E. Betzig, W. Wegscheider, L. Pfeiffer and K. West, Appl. Phys. Lett. **64**, 1421 (1994).

[5] C. L. Jahncke, H. D. Hallen and M. A. Paesler, J. of Raman Spectroscopy **27**, 579 (1996).

[6] F. Keilmann and R. Merz, Proceedings of NATO Advanced Research Workshop (ARW) on Near Field Optics, Acr-et-Senans, France, Kluwer **242**, 317 (1992).

[7] J.K. Trautman, E. Betzig, J. S. Weiner, D. J. DiGovanni, T. D Harris, F. Hellman and E. M. Gyorgy, J. of Appl. Phys. **71**, 4659 (1992).

[8] C.L. Jahncke and H.D. Hallen, Proceedings of 9th annual meeting of IEEE Lasers and Electro-Optics Society (LEOS) 96, **1**, 176 (1996).

[9] C.L. Jahncke, M.A. Paesler and H.D. Hallen, Appl. Phys. Lett. **67**, 2483 (1995).

[10] Randy X. Bain, Robert C. Dunn, X. Sunney Xie and P.T. Leung, Phys. Rev. Lett. **75**, 4772 (1995).

[11] X. Sunney Xie and Robert C. Dunn, Science **265**, 361 (1994).

[12] Eric Betzig and Robert J. Chichester, Science **262**, 1422 (1993).

[13] A. H. LaRosa, B. I. Yakobson and H. D. Hallen, Mater. Res. Soc. Symp. Proc. **406**, 189 (1995).

[14] A.H. LaRosa, B.I. Yakobson and H.D. Hallen, Appl. Phys. Lett. **70**, 1656 (1997).

[15] J. W. P. Hsu, M. H. Gray and Q. Xu, Proceedings of Defect Recognition and Image Processing in Semiconductors 1997. Proceedings of the Seventh International Conference on Defect Recognition and Image Processing in Semiconductors (DRIP VII). Institute of Physics Publishing, Bristol, UK; 1998; xx+524, 7-10 Sept. 1997; Templin, Germany, 27 (1998).

[16] J. W. P. Hsu, MRS-Bulletin **22**, 27 (1997).

[17] E.J. Ayars and H.D. Hallen, Appl. Phys. Lett. 76, 3911 (2000).

[18] E. J. Ayers, H.D. Hallen and C. L. Jahncke, Phys. Rev. Lett., **85**, 4180 (2000).

[19] Suzanne Huerth, Michael Taylor, Michael Paesler and Hans Hallen, Proceedings of the Second Asia-Pacific Workshop on Near-field Optics, Beijing, China, (1999).

[20] S. H. Huerth, M. P. Taylor, H. D. Hallen and B. H. Moeckly, Appl. Phys. Lett. 77, 2127 (2000).

[21] E. Betzig, A. Lewis, A. Harootunian, M. Isaacson and E. Kratschmer, Biophys. J. **49**, 269 (1986).

[22] D.W. Pohl, W. Denk and M. Lanz, Appl. Phys. Lett. **44**, 651 (1984).

[23] E. Betzig, P.L. Finn and J.S. Weiner, Appl. Phys. Lett. **60**, 2484 (1992).

[24] R. Toledo-Crow, P. C. Yang, Y. Chen and M. Vaez-Iravani, Appl. Phys. Lett. **60**, 2957 (1992).

[25] P.C. Yang, Y. Chen and M. Vaez-Iravani, J. Appl. Phys. **71**, 2499 (1992).

[26] B. I. Yakobson, A. LaRosa, M.A. Paesler, Ultramicroscopy **61**, 179 (1995).

[27] C.L. Jahncke and H.D. Hallen, Rev. Sci. Instr. **68**, 1759 (1997).

[28] J.W.P. Hsu, M. Lee and B.S. Deaver, Rev. Sci. Instr. **66**, 3177 (1995).

[29] Mark Lee, E.B. McDaniel and J.W.P. Hsu, Rev. Sci. Instr. **67**, 1468 (1996).

[30] J. W. P. Hsu, A. A. McDaniel and H. D. Hallen, Rev. Sci. Instr. **68**, 3093 (1997).

[31] R. Brunner, A. Bietsch, O. Hollricher and O. Marti, Rev. Sci. Instr. **68**, 1769 (1997).

[32] Khaled Karrai and Robert D. Grober, Appl. Phys. Lett. **66**, 1842 (1995).

[33] M.J. Gregor, P.G. Blome, J. Schöfer and R.G. Ulbrich, Appl. Phys. Lett. **68**, 307 (1996).

[34] Igor I. Smolyaninov, Walid A. Atia, Saeed Pilevar and Christopher C. Davis, Ultramicroscopy **71**, 177 (1998).

[35] C. L. Jahncke, S. H. Huerth, Beverly Clark III and H. D. Hallen submitted.

[36] Chad E. Talley, Gregory A. Cooksey and Robert C. Dunn, Appl. Phys. Lett. **69**, 3809 (1996).

[37] Din Ping Tsai and Wen Rei Guo, J. Vac. Sci. Technol **A15**, 1442 (1997).

[38] Michael Muto, "High throughput, high input power probe for IR near-field scanning optical microscopy," M.S. Thesis, North Carolina State University, (1997).

[39] P.K. Wei and W.S. Fann, J. Appl. Phys, **83**, 3461 (1998).

[40] K. Karrai and I. Tiemann, Phys. Rev. B, **62**, 13174, (2000)

[41] Chih-Chun Wei, Pei Kuen Wei, and Wunshain Fann, Appl. Phys. Lett. **67**, 3835 (1995).

[42] K.E. Fellows, C.L. Jahncke, E.J. Ayars and H. D. Hallen, unpublished.

[43] R. M. Pashley and J. A. Kitchener, J. Colloid and Interface Sci., **71**, 491 (1979).

[44] R.G. Horn and J. Israelachvili, J. Chem. Phys., **75**, 1400 (1981).

[45] P.K. Wei and W.S. Fann, J. Appl. Phys., **87**, 2561 (2000).

[46] P.M. Wiggins, Microbiol. Rev., **54**, 432 (1990).

Figure Captions

Figure 1: Time-traces of the vertical tip position over the sample showing the asymmetry of the oscillation where the sample is closest to the probe at the bottom of the figure.

Figure 2: (a) Resonance curves obtained with the tuning fork method of oscillation amplitude measurement with a quality factor of approximately 600. These curves shift and broaden as the feedback setpoint is decreased (85%, 75%, 65%, 50%) moving the probe closer to the surface. (b) the resonance curves obtained using the mathematical model for various values of xc (86%, 75%, 63%, 56%) reported in a percent of the free oscillation amplitude.

Figure 3: The gain of the system is increased until there are oscillations of the type we see in figure 1. In this graph these oscillations are monitored as a function of drive frequency without further adjustment of the gain and are plotted as diamonds. The resonance curve is shown as a solid line and is overlaid for reference. As the time response of the system improves, the oscillation amplitude decreases as can be seen on either side of the resonance curve.

Figure 4: The time response of the probe due to a pulse on the z-piezo as a function of driving frequency, which is indicated by the overlaid resonance curve. The outward motion is the black curve, which is in response to the inward pulse. The inward motion is the gray curve, which is in response to the outward pulse..

Figure 5: The feedback response to an 8msec ramp function on the z-piezo for a variety of driving frequencies on either side of the resonant frequency. The gain is optimized for each driving frequency so that there is no overshoot as seen in figure 3. The black lines are the outward motion. The gray lines are the inward motion. The resonance curve is overlaid for reference.

Figure 6: (a) The experimental time response for the probe to find the surface with optimized gain given an 8msec ramp step as seen in figure 5. (b) the numerical calculation of the time response for the feedback signal to drop to 1/e for a variety of driving frequencies for two situations: turning the tapping off and turning the tapping on. This time response is overlaid with the resonance curve for reference in both (a) and (b).

Figure 7: Numerical resonance curves for three different resonance frequencies, 39524 Hz, 35931 Hz, and 32328 Hz normalized to 35931 Hz. The undamped resonance curves and the resonance curves damped to 85% are shown. The three resonance curves are essentially indistinguishable.

Figure 8: Numerical resonance curves for two Quality factors, 630 and 315, where the frequency axis is normalized to show the differences as the setpoint is decreased.

Figure 9: The results of the numerical model showing the 1/e time response for the system to settle after turning the tapping perturbation on and off for two different Q

values, 630 and 315. The frequency axis is normalized so that the undamped resonance curves for the two Q values are aligned.

Figure 10: Approach curves for two different fiber/fork oscillation amplitudes where the fiber is pulled away from a surface that is tilted ~24° forming an angle between the probe and the fiber of ~66°. The approach curves for both oscillation amplitudes have two distinct regions of interest, A and B, where the feedback signal changes slowly and then rapidly with distance from sample, respectively.

Figure 11: Experimental resonance curves showing the undamped resonance, a resonance at 35% of the free resonance and a clamped resonance curve. The peak of the clamped resonance is only 2% of the undamped resonance peak, and the frequency shift is ~400Hz.

Figure 12: As the setpoint is decreased, the resonance curve shifts to a higher frequency. This peak shift as a function of a fraction of the resonance peak amplitude is shown for the same two cases as seen in figure 10: the sample is tilted 24° and the probe is given two different oscillation amplitudes. The lines are to guide the eye and indicate two different regions of peak shift where the peak starts out shifting slowly (a few Hz) and then begins to shift rapidly (10's of Hz).

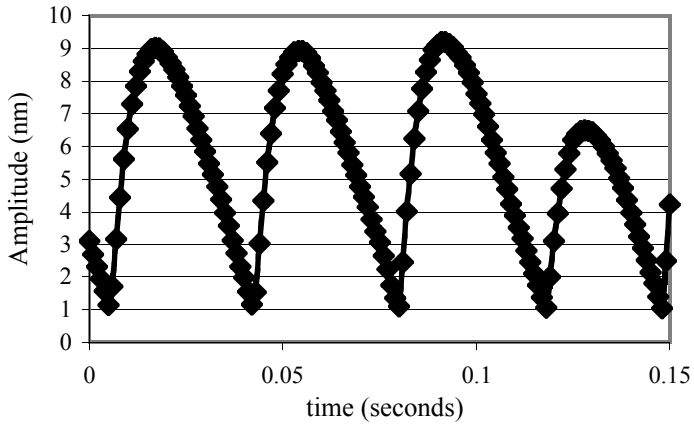

Figure 1

Jahncke and Hallen

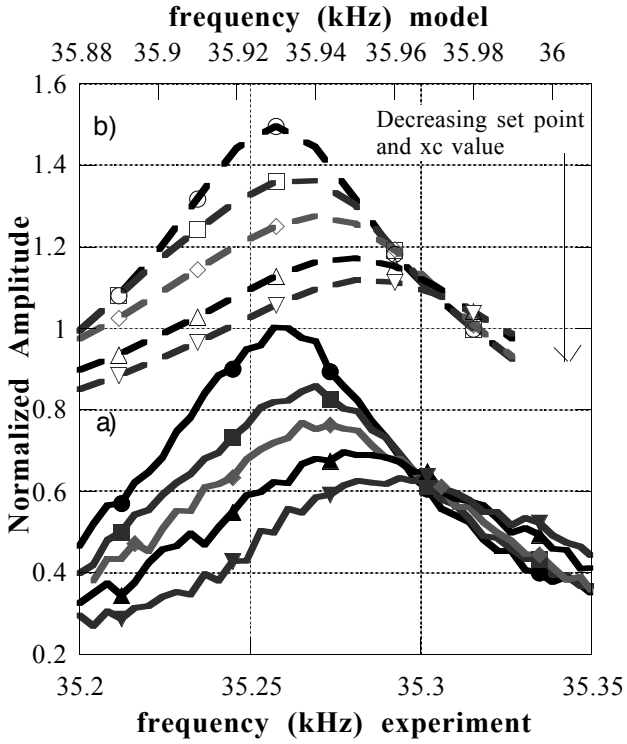

Figure 2 a) and b)

Jahncke and Hallen

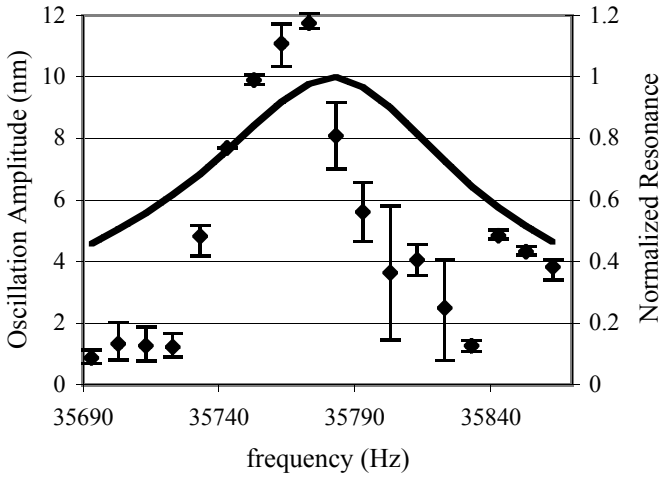

Figure 3

Jahncke and Hallen

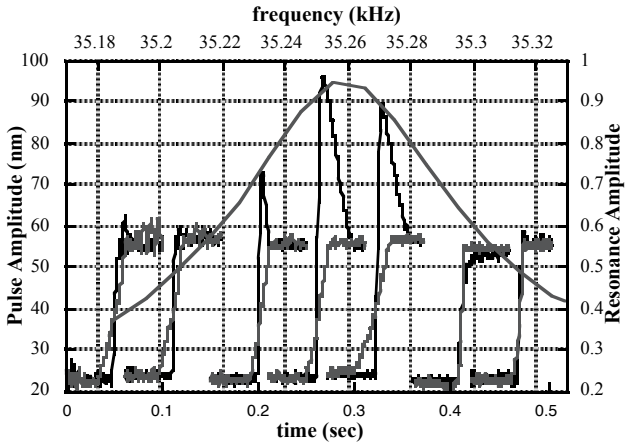

Figure 4

Jahncke and Hallen

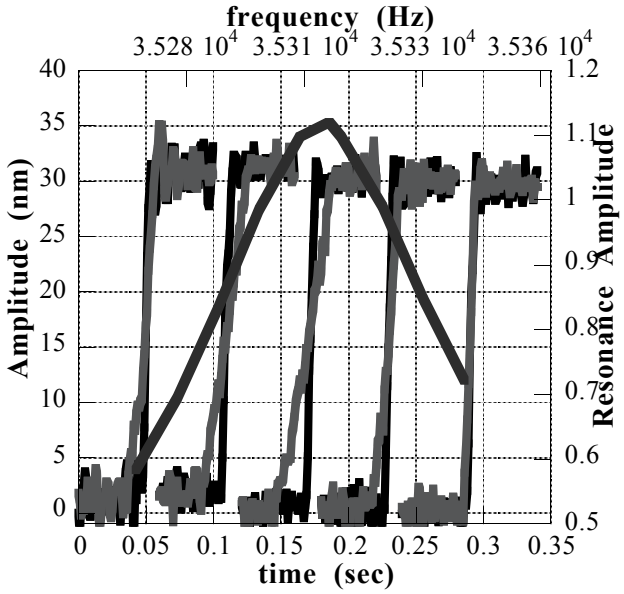

Figure 5

Jahncke and Hallen

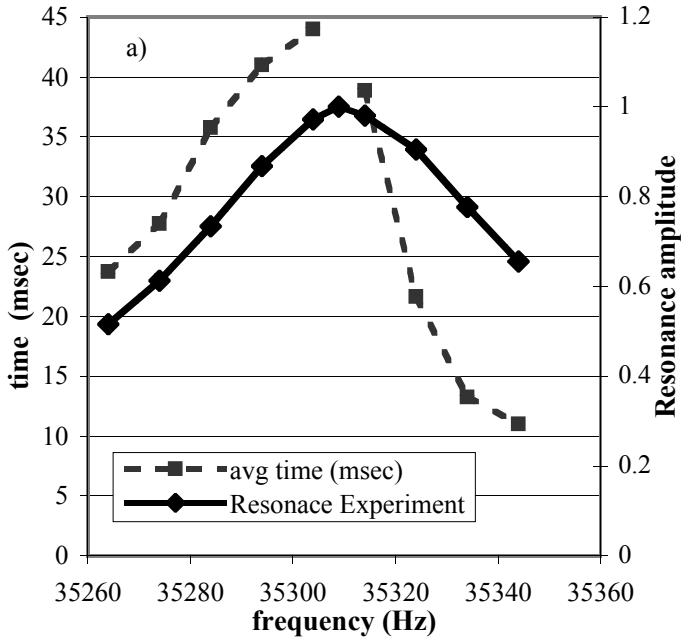

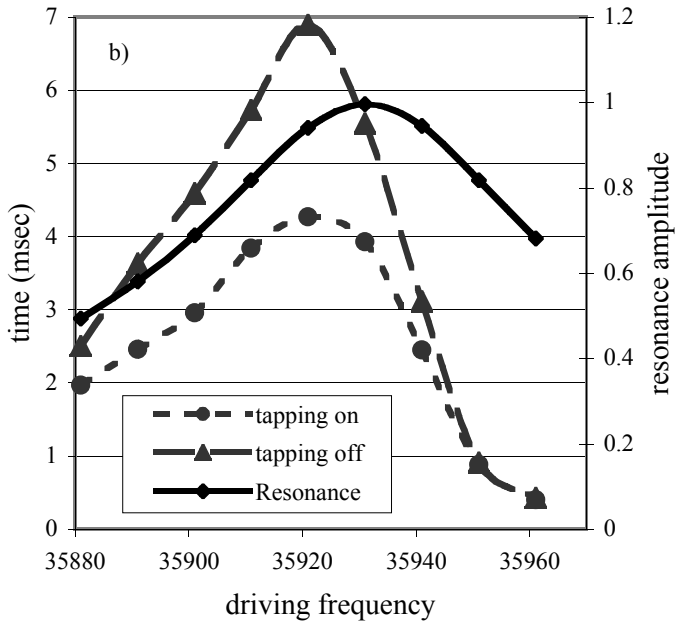

Figure 6

Jahncke and Hallen

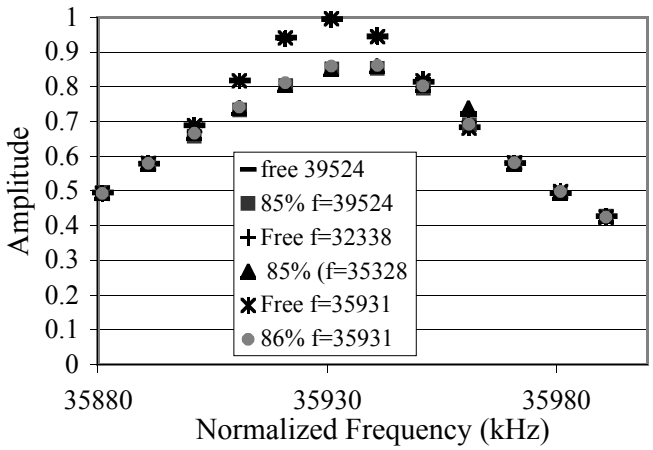

Figure 7

Jahncke and Hallen

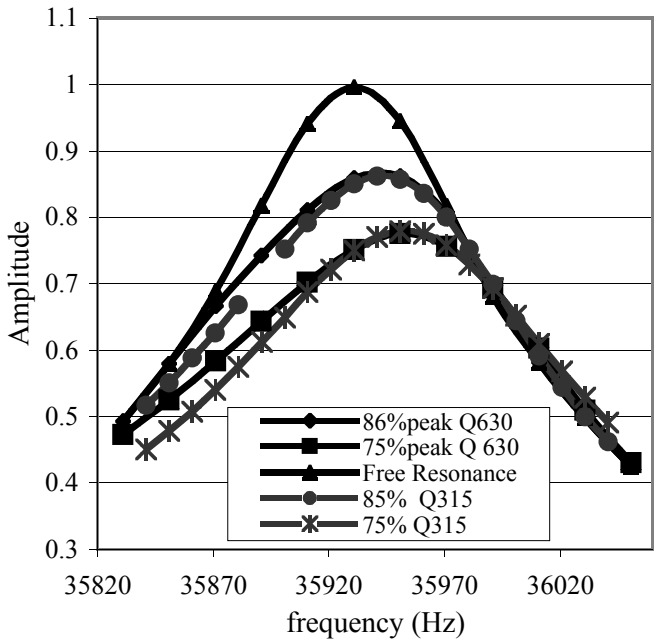

Figure 8

Jahncke and Hallen

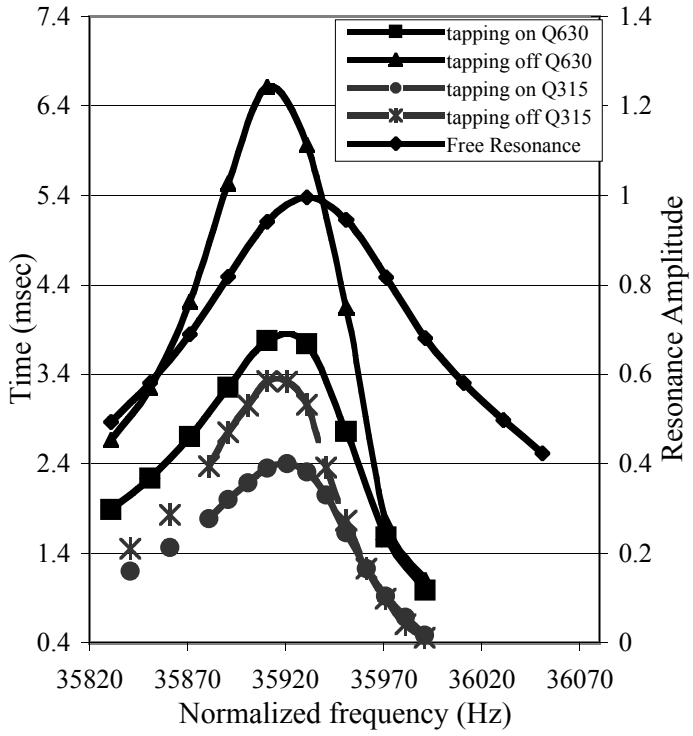

Figure 9

Jahncke and Hallen

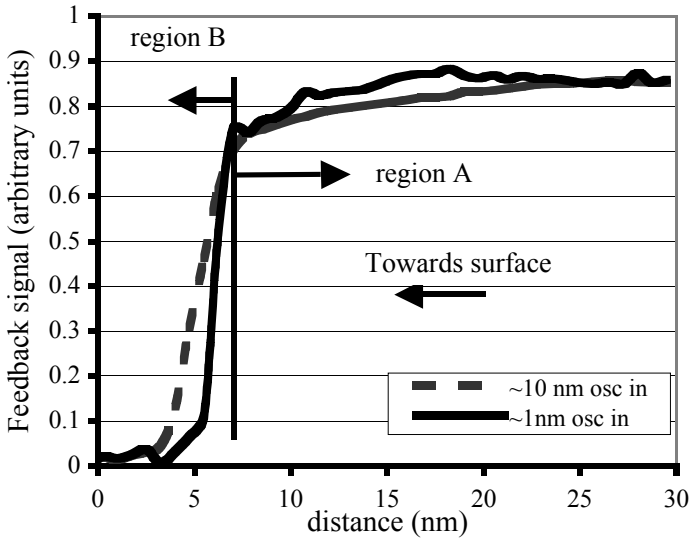

Figure 10

Jahncke and Hallen

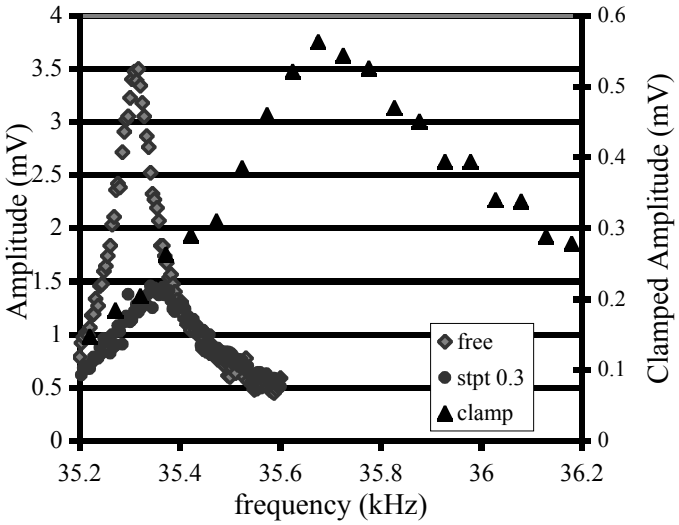

Figure 11

Jahncke and Hallen

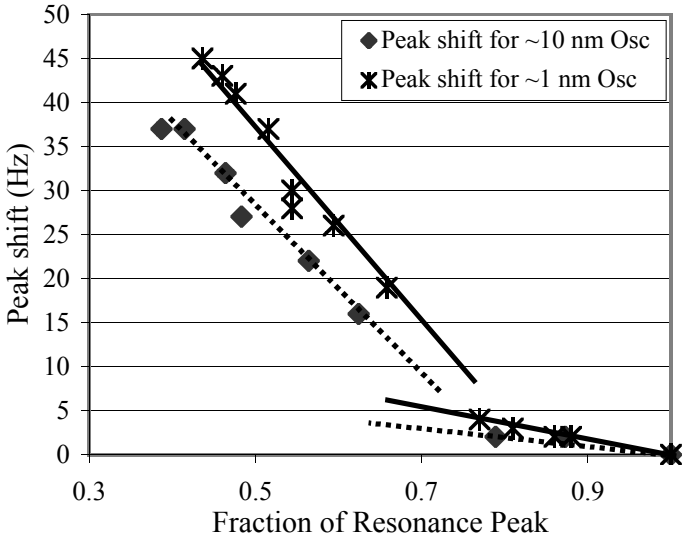

Figure 12

Jahncke and Hallen

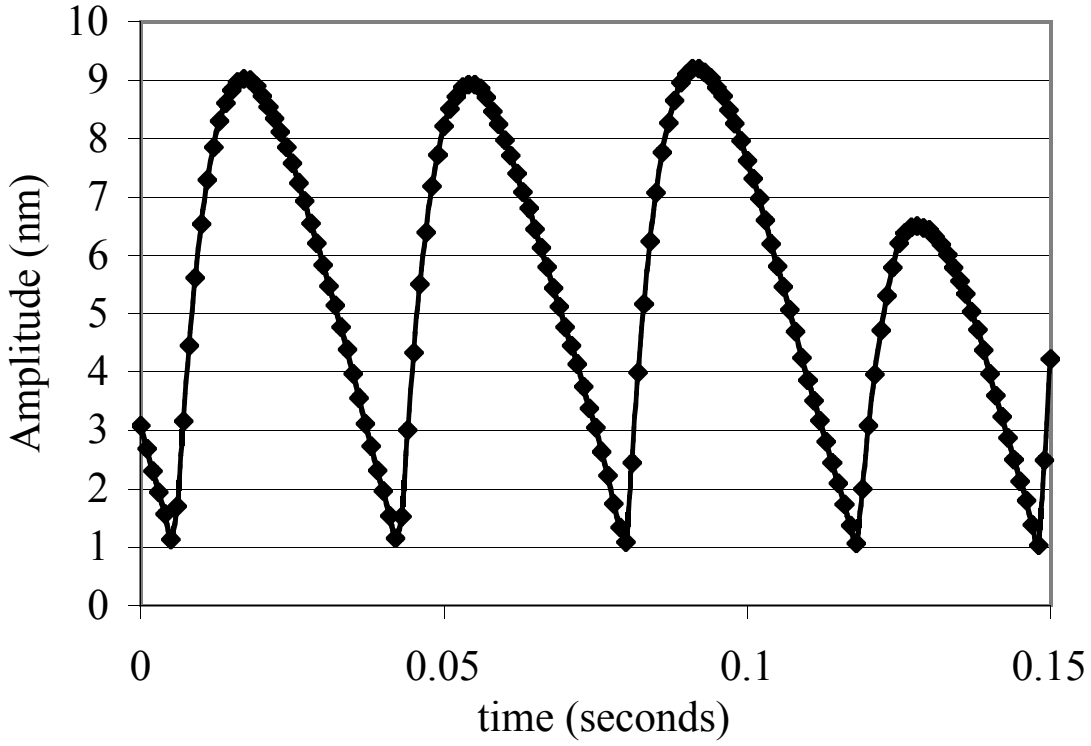

Figure 1

Jahncke and Hallen

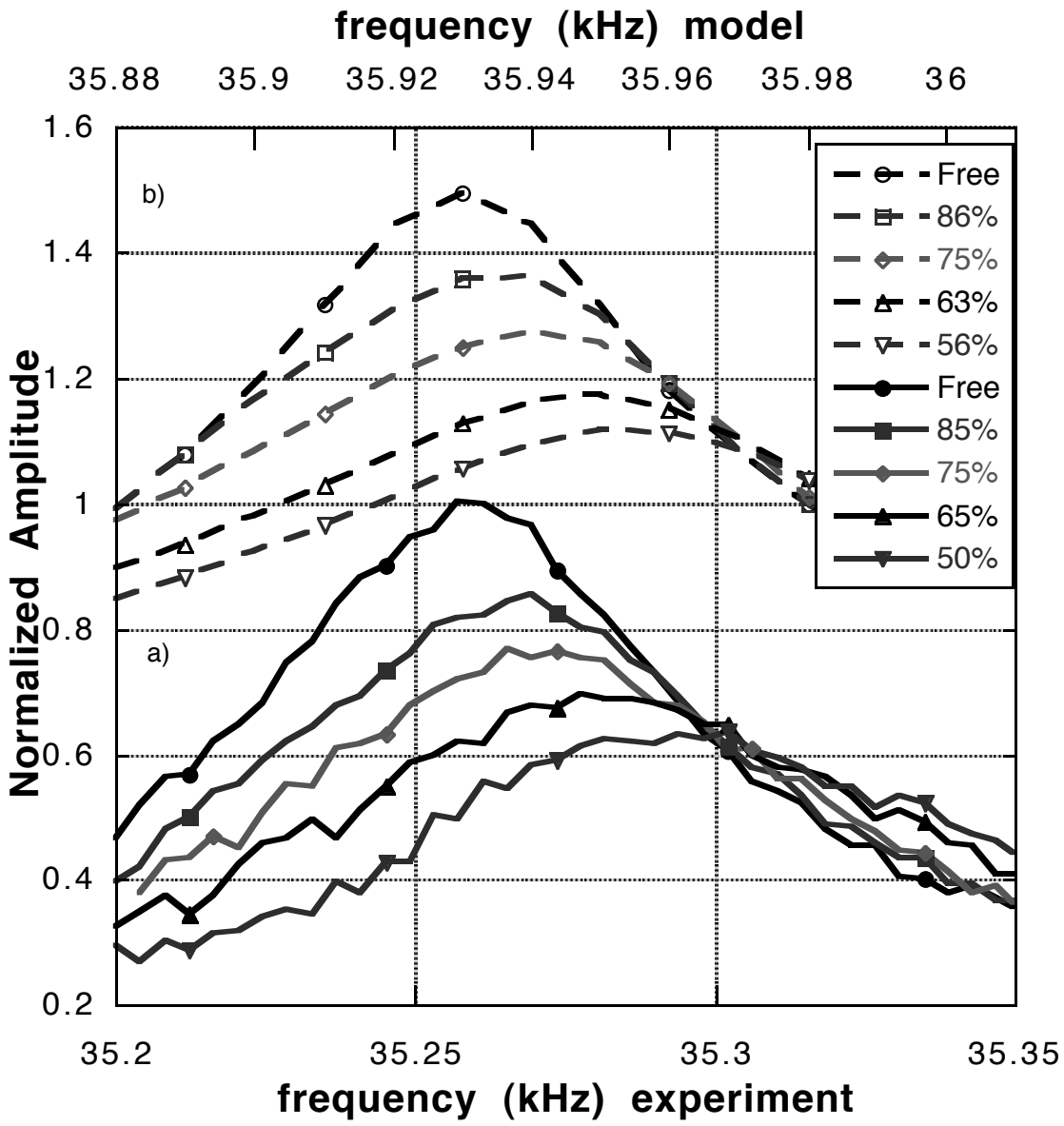

Figure 2 a and b

Jahncke and Hallen

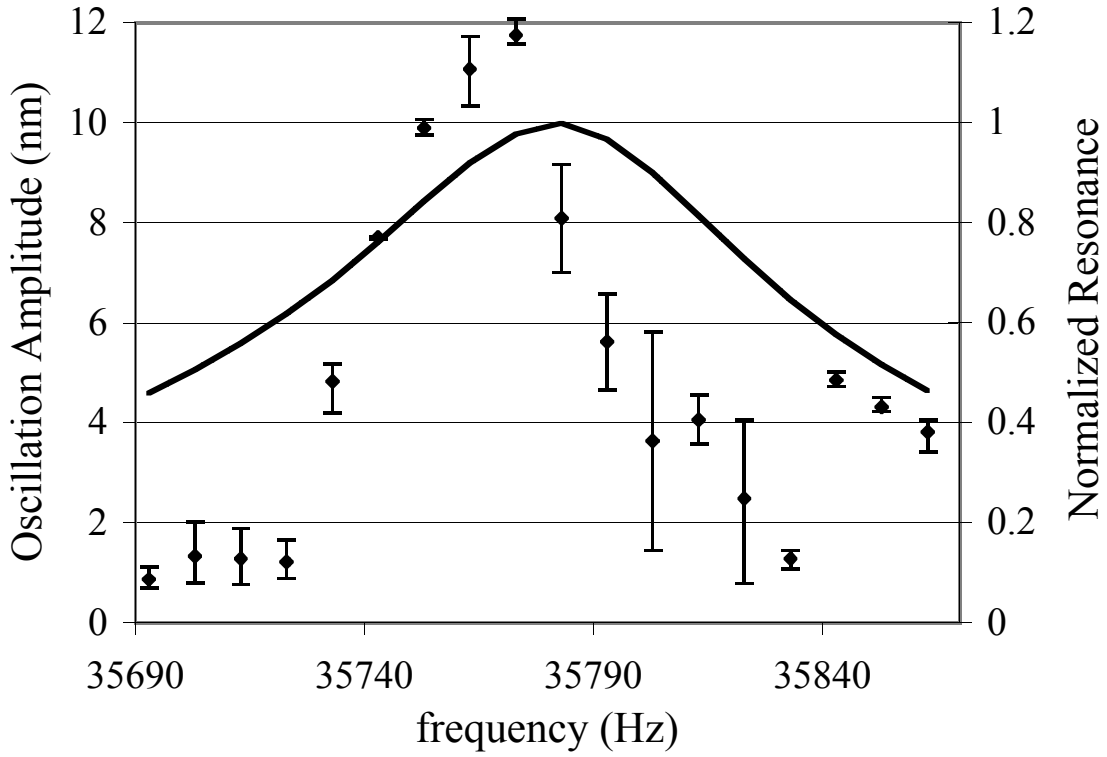

Figure 3

Jahncke and Hallen

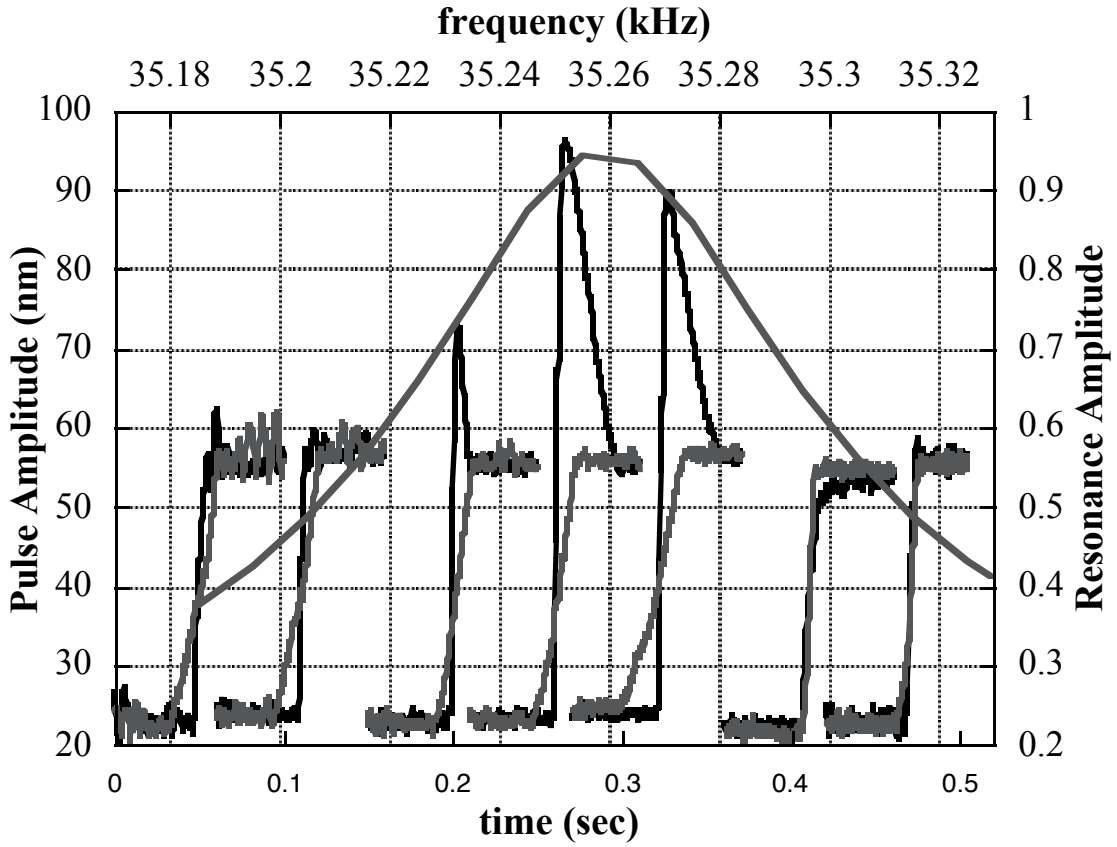

Figure 4

Jahncke and Hallen

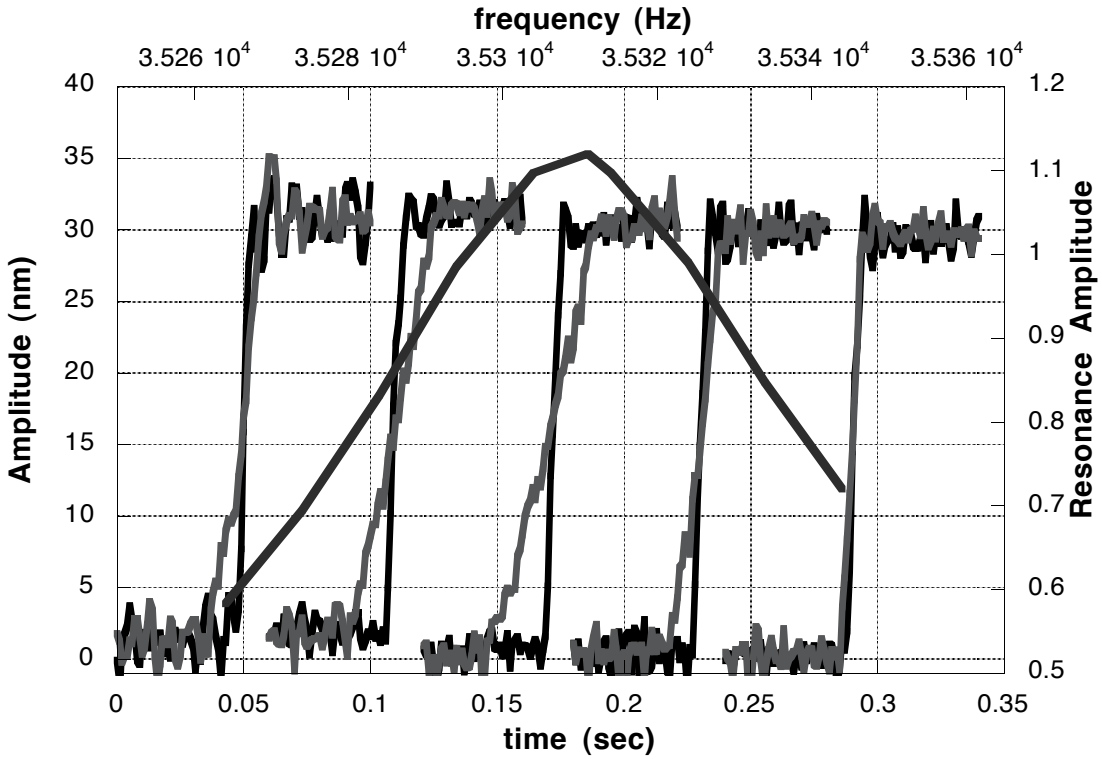

Figure 5

Jahncke and Hallen

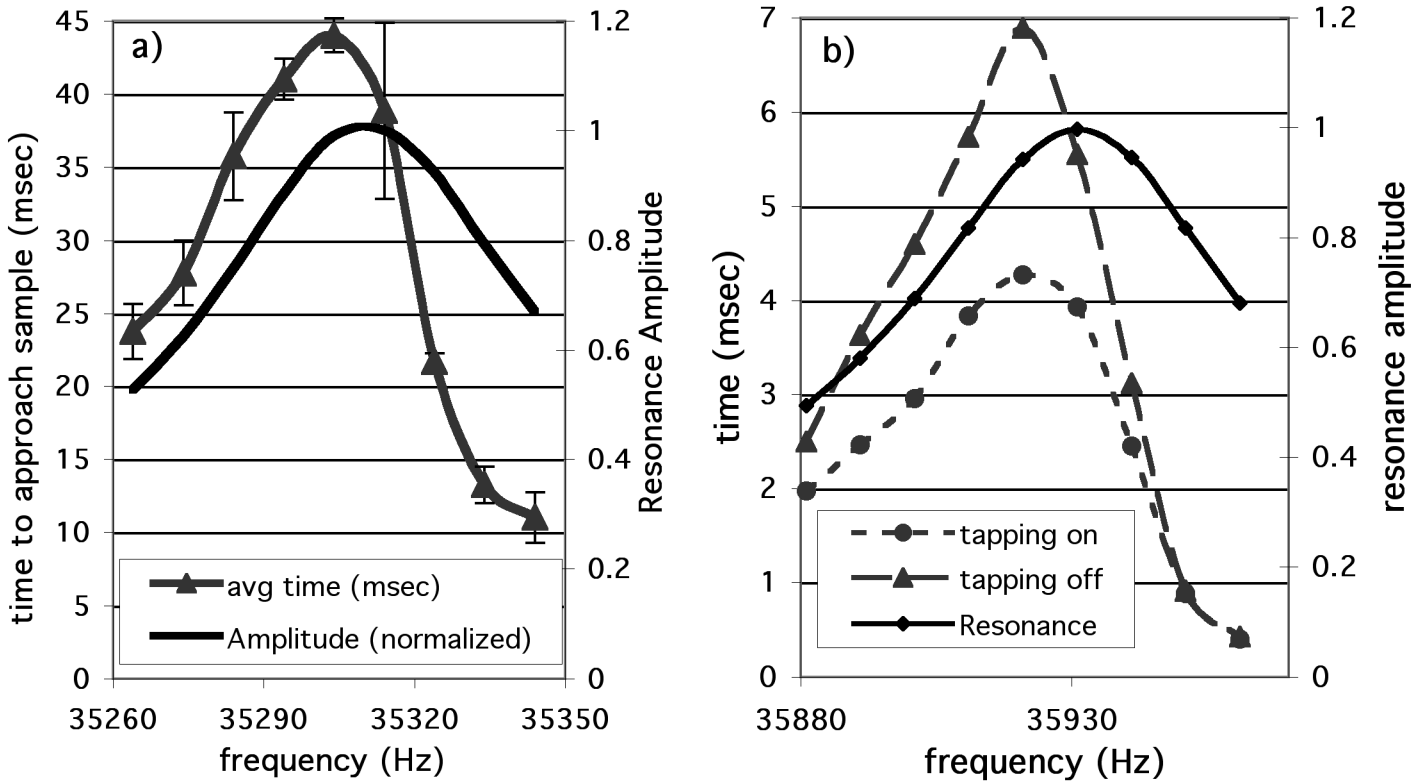

Figure 6 Jahncke and Hallen

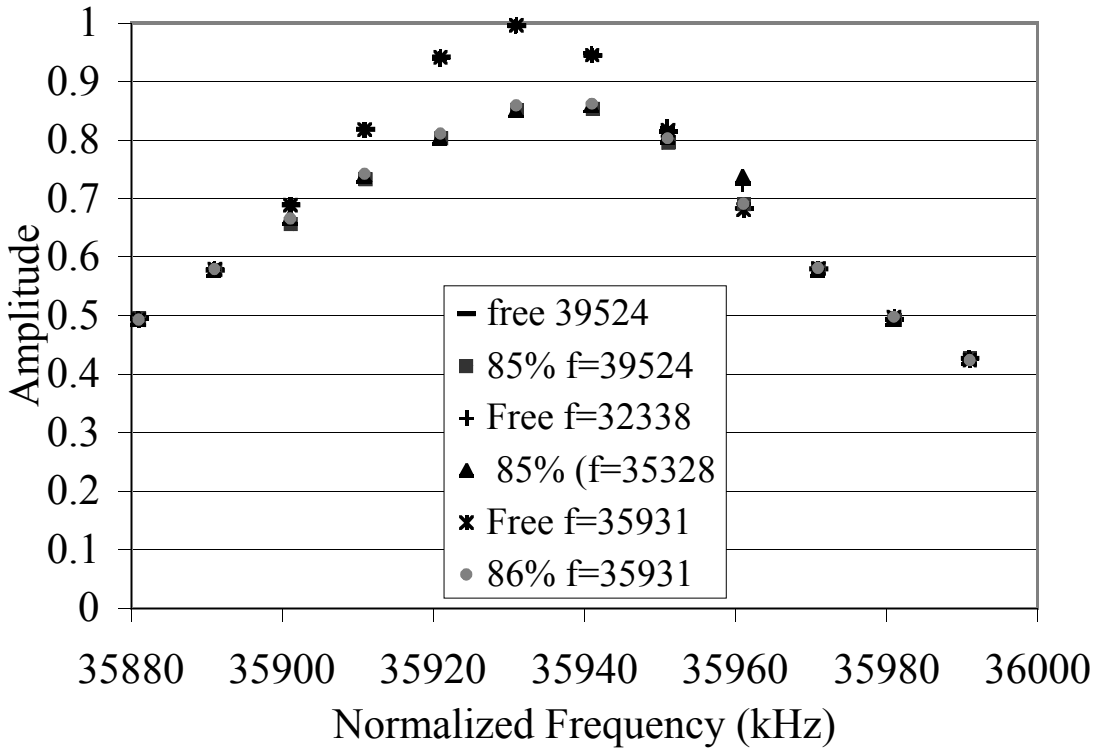

Figure 7

Jahncke and Hallen

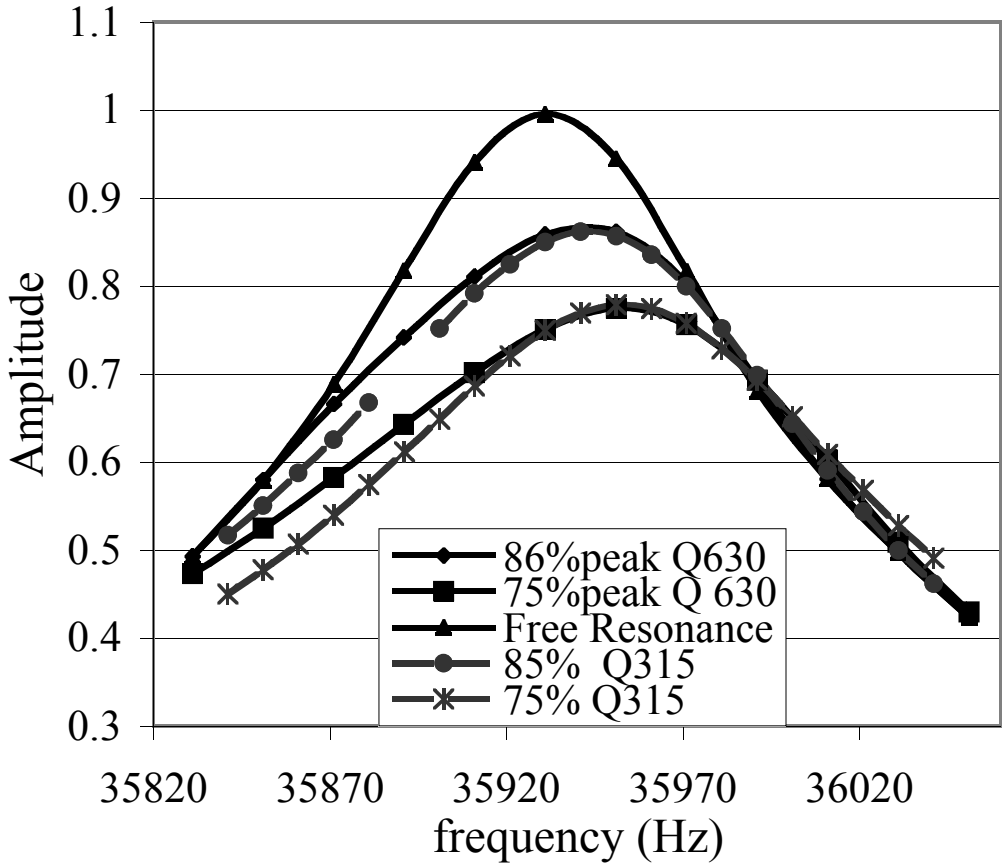

Figure 8

Jahncke and Hallen

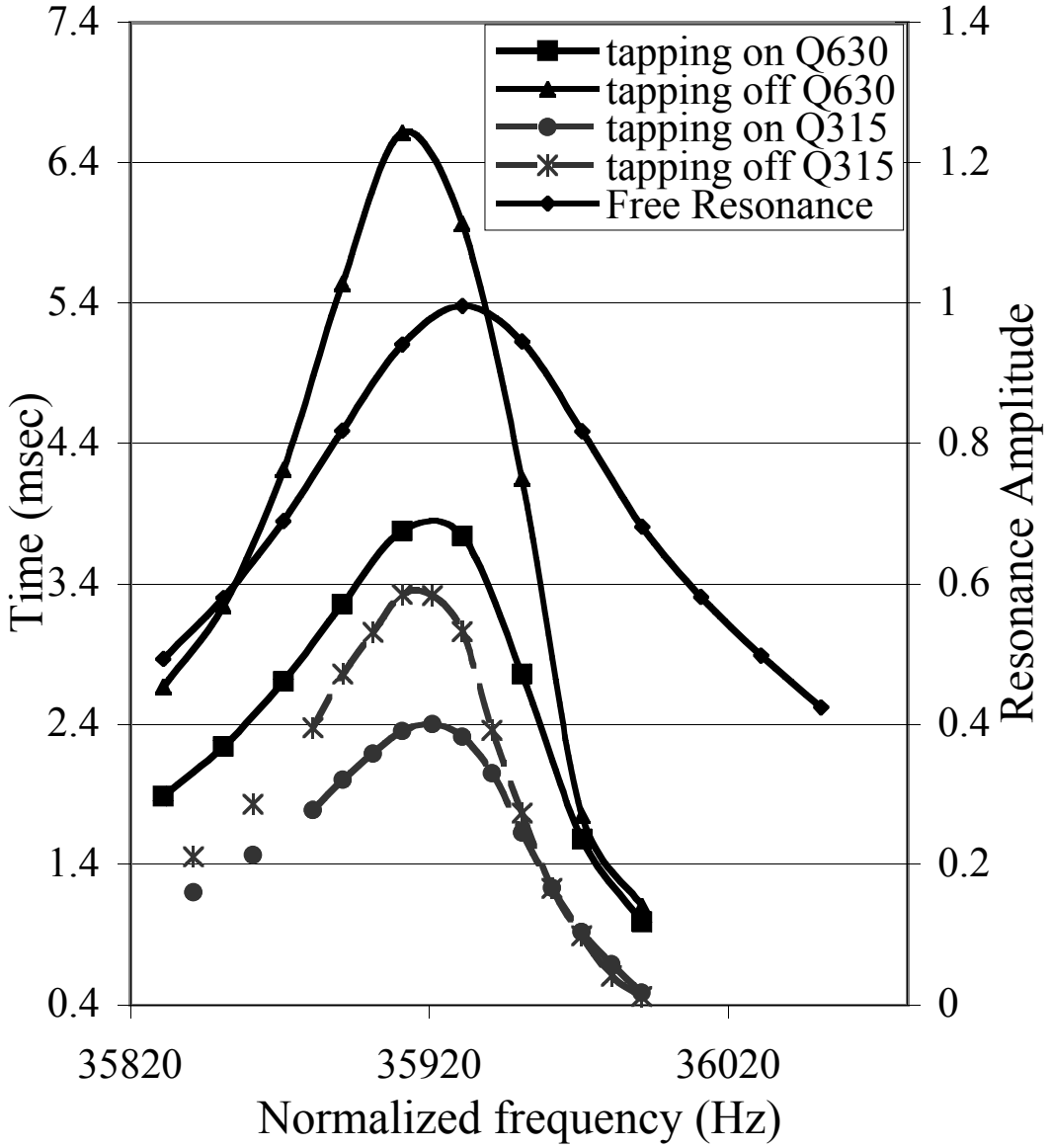

Figure 9

Jahncke and Hallen

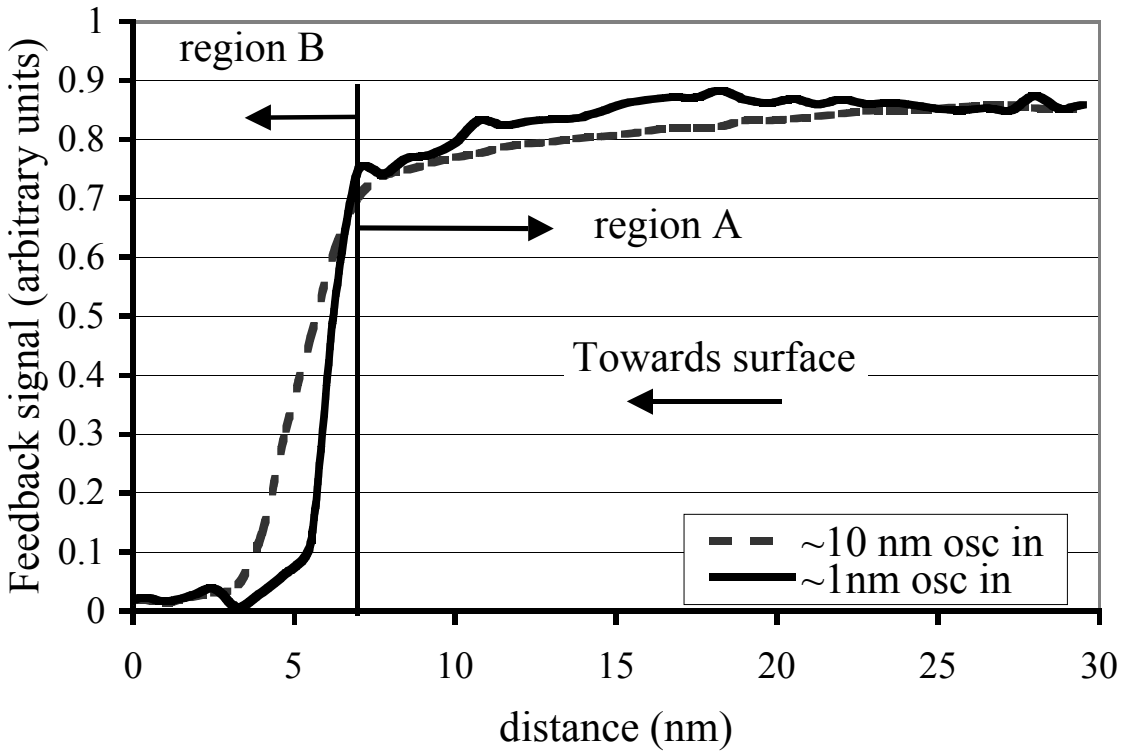

Figure 10 Jahncke and Hallen

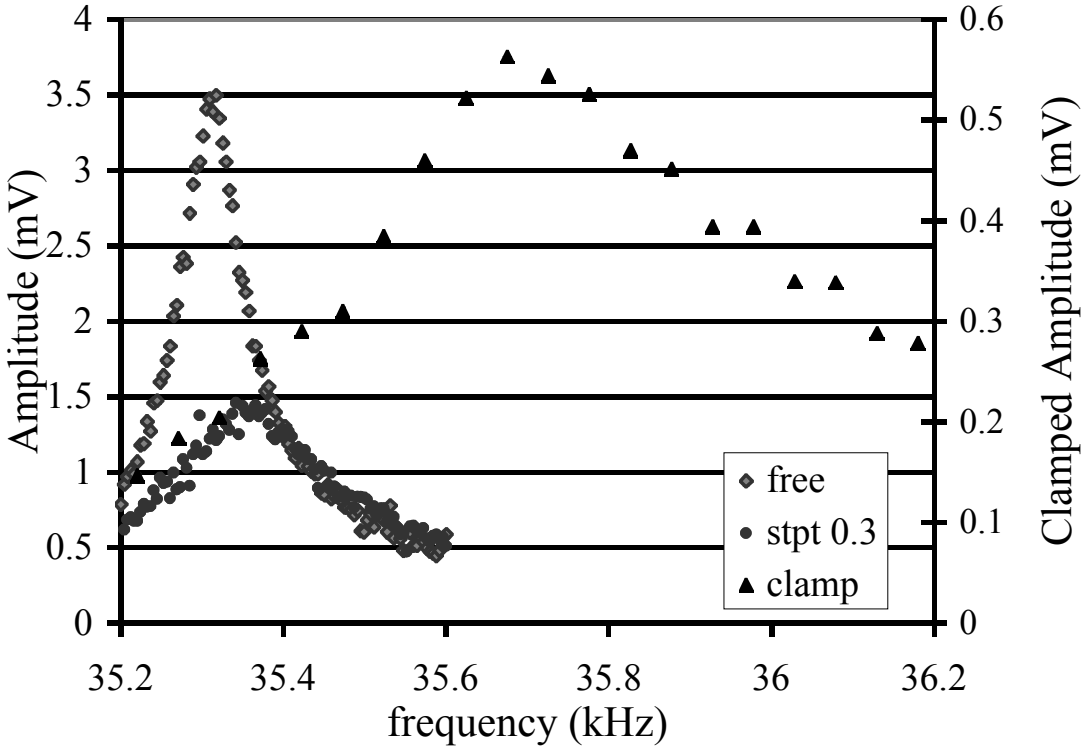

Figure 11 Jahncke and Hallen

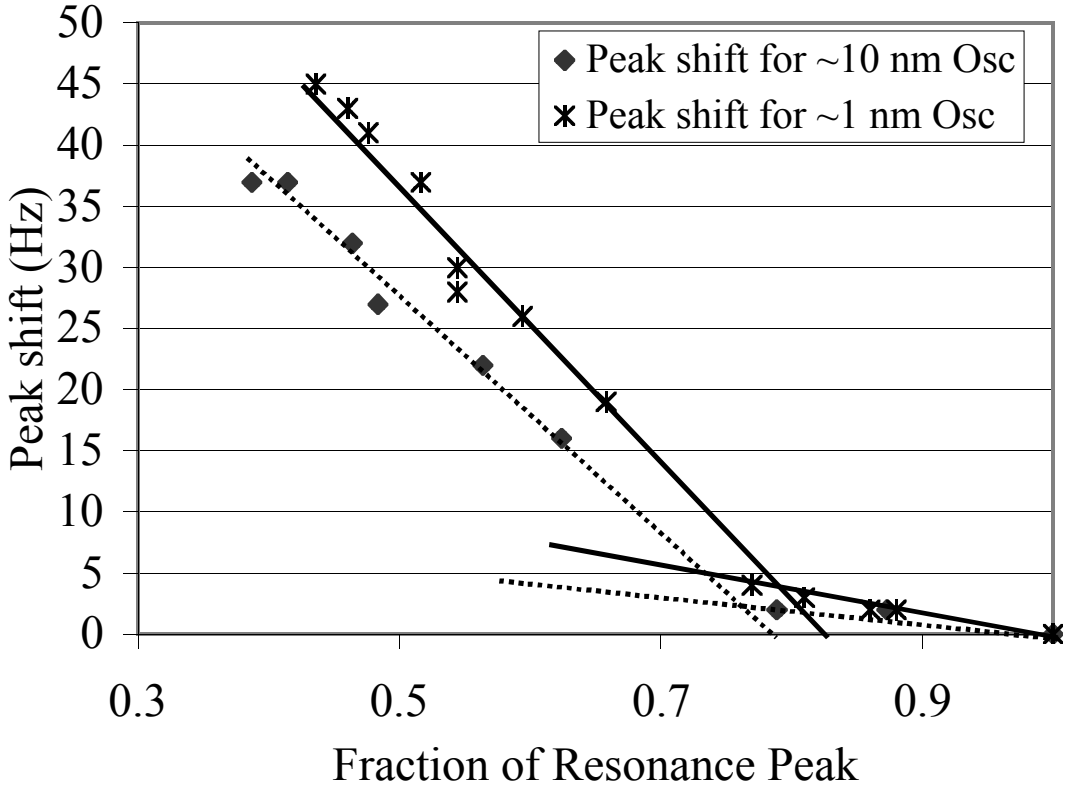

Figure 12

Jahncke and Hallen